

Experimental Determination of Drag Coefficient on Different Automobiles Geometry

Dr.Abdulhassan A.Karamallah  & Dr.Abdessamed Kacem Wahab*

Received on: 15/12/2009

Accepted on: 6/10/2011

Abstract

The undertaken research deals with an experimental determination of drag coefficient for five car models. Experiments were run within a subsonic aspiration wind tunnel, covering an air speed up to 33m/s. Drag coefficients of 0.45, 0.39, 0.53, 0.34 and 0.68 for Mercedes SEL300, Hyundai, Toyota, Pajero, and Mini-Bus models were obtained respectively.

The flow field around the pre-quoted models with a qualitative description about the flow visualization for car models using a subsonic smoke wind tunnel has been accomplished.

Keywords: Aerodynamic of automobile, Drag coefficient, Strain gauge.

التحديد التجريبي لمعامل الكبح على نماذج سيارات ذات أشكال هندسية مختلفة

الخلاصة

يتناول البحث الحالي التحديد التجريبي لمعامل الكبح لخمسة نماذج من المركبات. أجريت التجارب داخل نفق هوائي قليل السرعة (دون سرعة الصوت) مغطياً مدى سرعة الهواء يصل الى 33 متر/ثانية. أرقام معامل الكبح لنماذج مركبات تحاكي مرسيدس SEL300، هيونداي، تويوتا، باجيرو، ونموذج باص صغير كانت كالاتي: 0.45 ، 0.39 ، 0.53 ، 0.34 ، و 0.68 على التوالي.

مجال الجريان حول النماذج المذكورة مع تصور نوعي حول مشاهدة أسلوب الجريان لهكذا أنواع من المركبات تم باستخدام نفق هوائي واطيء السرعة مزود بمولد دخان .

1. Introduction

Up to now the improvements in aerodynamics have mainly been accomplished by improvements in the shape of the upper body of the vehicle. Even if some limitations have been anticipated in the maximum allowed velocity for the future vehicles the aerodynamic drag for a modern car, model year 1999, at 80 km/h constitute approximately 50% of the total driving resistance [1]. For a modern car the basic shape stands for approximately 45%, wheels and

Wheel-housing for 30%, the floor and detailing for 25% of the total drag [2]. The flow in the underbody region is complex partly due to the geometry of the underbody and partly due to the interaction between the vehicle and the ground. One of the major drag contributors in this region is the wheel [3]. As been shown by reference [4], the major part of the drag comes from the part of the wheels and only a minor part originates from the wheel-openings. Streamlining of the underbody would summarize to around 0.17 in decreasing the Cd.

Reference [5] also makes it clear that the underbody flow is the next topic for automotive aerodynamics. Reference [6] did a study of how drag and lift is affected by under body diffusers. This study was continued in reference [7] where a complete moving ground study has been done. Reference [8] shows however that the rear wheel wake drastically decreases the diffuser Efficiency which makes it hard to trust a tool based on data from a simplified geometry. Reference [9] claims that moving floor and rotating wheels leads to a reduction in flow angularity at the front wheels. Reference [10] have done some work on the aerodynamically development within a car project at Volvo. It is mentioned that underbody add on features that reduces drag have twice as large effect in the DNW wind tunnel with moving floor capabilities then what is a fact in the Volvo wind tunnel. It is also stated that this effect is different for other types of cars. Reference [11] concluded that drag is mainly improved by reducing the ground clearance and the wheel housing size, or by increasing the track. Reference [12] presented the optimization result, the effect of vortex generators in the flow field and the mechanism by which these effects take place. The automotive underbody flow characteristics were simulated by reference [13] for a 20% scaled car model, where different underbody shapes were designed. Main influence factors which affect coefficient of aerodynamic lift are cavity of wheel and wheel in turn, and the

influences of vent-pipe groove and shapes are small.

Current work shows however that the number of shape of the upper body of the vehicle affects the drag on a vehicle.

2. The Experimental Apparatus

2.1 The Wind Tunnel

The wind tunnel used in the present work is EA600 Delta-Lab, aspiration type with a squared test section of 230mm×230mm and maximum velocity of 35m/s (Sited at Houari Boumediene University for Science & Technology in Algeria). It is made from rigid PVC and air is drawn in, throughout the convergent diffuser. The squared test section is made from transparent altuglass. The test section upper wall is provided with 7 waterproof holes in order to enter the Pitot tube. The diffuser is connected with the ventilator by an elastic connector in order to keep it away from the external vibrations that are produced by motor-ventilator group. The centrifugal ventilator is fixed over an independence frame, and it is controlled by an electronic frequency variator [14]. Figure (1) shows the main parts of the wind tunnel. The wind tunnel is provided with one Pitot tube and displacement system in depth of the test section. It is also provided with one multi-manometer EI 104 (24 tubes of 500 mm height).

Pressure measurements are carried out with the aid of Pitot tube with a holder which permits for moving it through the depth of the test section.

2.1.1 Wind Tunnel Calibration

The calibration of wind tunnel test section was carried out and the gained results showed a uniform velocity distribution within the working section. The velocity distribution at the test section is shown in figure (6).

2.2 Extensometer Bridge

The extensometer bridge which was used in the present work to measure the aerodynamic forces six channels Delta-Lab EI 616 type issued to measure the deformations of the strain gauges. It consists of one digital indicator of 20000 points, potentiometers for initial balance of gauges, and one adjuster (regulator) among 1 and 5 of the gauge factor, [15]. Strain gauges are connected in a half-bridge connection type as shown in figure (2).

2.3 The Tested Models

Five models are shown in figure (3), reproducing three, two, and one-box form passenger cars made from the PVC, hardwood, and steel with different scales, were tested. Mercedes model with a scale of 1/20 and a blockage ratio of 16% as well as to Hyundai model with a scale of 1/30 and a blockage ratio of 2.5% reproduce three-box form passenger car type. Toyota model with a scale of 1/20 and a blockage ratio of 16% as well as to Pajero model with a scale of 1/30 and a blockage ratio of 2.5% reproduce two-box form passenger car type. SNVI Mini-Bus model with a scale of 1/40 and a blockage ratio of 8.4% reproduces one-box form passenger car type.

3. Experimental Calculations

Five pre-quoted models were tested. Each model was fixed at the end of the sting by a stud and nut, as shown in figure (4). The sting is made of a hot rolled medium Carbon steel (0.45%C) with a Young modulus of elasticity ($E=203.4 \times 10^9 \text{N/m}^2$) and a cross section $b \times h$ of $(12.6 \times 5.16)10^{-3} \text{m}$.

Dimensions of the sting were chosen so as to reproduce a minimum strain that it can be read via the strain gauges. Each model was fixed at the reference point of the sting. The bending moment is given by,

$$M_O = F_Y \cdot X_C + F_X \cdot Y_C \quad \dots(1)$$

The value of $(F_Y \times X_C)$ approaches to zero (Direct strain which is due to the effect of F_Y in the range of 0.3% of the total strain as a reason of F_X and M_o effect) [16]. The two equations to find two unknowns (M_o and F_X) can be obtained by sting vertical position. The model and four strain gauges were fixed at the reference point (O), (B), and (A) as shown in figure (5-a). L_a represents the distance of strain gauges (A) from the reference point (O). L_b represents the distance of strain gauges (B) from the reference point (O). From the bending moment diagram shown in figure (5-b),

$$M_A = M_O + F_X \cdot L_a \quad (2)$$

and

$$M_B = M_O + F_X \cdot L_b \quad (3)$$

M_A, M_B have a direct relation with the readings of strain gauges ϵ_A and ϵ_B , respectively, according to the subsequent equations:

$$\begin{aligned} \epsilon_A &= \sigma_A / E = M_A \cdot h / 2I_Z E \\ \text{or } M_A &= 2I_Z E \epsilon_A / h \\ \text{and } \epsilon_B &= \sigma_B / E = M_B \cdot h / 2I_Z E \end{aligned} \quad (4)$$

$$\text{or } M_B = 2I_Z E \epsilon_B / h \quad (5)$$

Where I_Z represents the second moment of area for the sting around the z-axis. The solution of equations (2) and (3) identifies the values of the unknowns, F_X and M_o . The drag coefficient is given according to the known relation:

$$C_D = F_X / 0.5 \rho V_\infty^2 A_f \quad (6)$$

Fluid velocity (air-speed) could be estimated by Bernoulli's Equation.

In order to identify the relative error, Bernoulli's equation can be written as

$$dV/V = 0.5 dH/H$$

Where dH is the absolute error ratio in total pressure head expressed by:

$$dH = \sqrt{(H - H_m)^2 + (dH)^2}$$

Where H represents the total head.

The deviation analysis for drag force measurements are obtained from equations (4) and (5),

$$M_A = C_1 e_A$$

and $M_B = C_1 e_B$

Where $C_1 = 2I_Z E / h$

By substituting in equations (2) and (3) yields,

$$C_1 d e_A = d M_O + L_a d F_X \quad (2a)$$

$$C_1 d e_B = d M_O + L_b d F_X \quad (3a)$$

From the two equations (2a) and (3a),

$$\ln F_X = \ln(e_A - e_B)$$

or

$$dF_X / F_X = \pm \sqrt{(d e_A / e_A)^2 + (d e_B / e_B)^2}$$

Since

$$G.F = (\Delta R / R) / e \quad (8)$$

$(\Delta R / R)$ is considered as constant since it includes the strain approximation:

$$\delta G.F / G.F = -\delta e / e$$

or $\delta e = (\delta G.F / G.F) \epsilon \quad (9)$

The deviation of drag coefficient will be obtained from the equation,

$$dC_D / C_D = (dF_X / F_X) - (2dV/V) = \pm \sqrt{(dF_X / F_X)^2 + (2dV/V)^2} \quad (10)$$

4. Results and Discussion

Figure(7) shows the direct relation of strain readings at strain gauges A and B, with an air speed for models Mercedes SEL300, Hyundai, Toyota, Pajero and SNVI Mini-Bus, respectively.

Drag coefficient variation as a function Reynolds number for different vehicles' profiles were presented in figure (8).

Deviation errors for mentioned five models are shown in figure (9). It is noted that high readings of strain leads to high accuracy in measured values.

5. Conclusions

The major conclusion from present work can be listed as follows:

Results of C_D , using the strain gauge method, are extremely encouraging. This method is, therefore, a viable investigation tool that can be used to determine the drag coefficient for automobiles.

6. Notations

A_f : The model frontal area (m^2)

C_D : Drag Coefficient

E : Young modulus of Elasticity (N/m^2)

F_X : Total Drag Force (N)

F_Y : Lift Force (N)

h : Thickness of beam (m)

I_Z : Second moment of area (m^4)

L_a : The distance of strain gauge A from

The reference point (O).

L_b : The distance of strain gauge B from

The reference point (O).

M_A : Moment at A (N.m)
 M_B : Moment at B (N.m)
 (X_C, Y_C) : Centroid of beam
 V_∞ : Undisturbed air flow (m/s)
 ϵ_A : Strain at strain gauge A (μ strain)
 ϵ_B : Strain at strain gauge B (μ strain)
 ρ : Air density (kg/m^3)
 σ_A : Stress at A (N/m^2)
 σ_B : Stress at B (N/m^2)

References

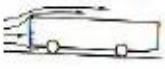
- [1] Hucho W.-H., 'Aerodynamic of road vehicles', SAE, ISBN0-7680-0029, 1998.
- [2] Carr G. W., 'New MIRA drag reduction prediction method for cars.' Automotive Engineer, June/July, 1987.
- [3] Mercker, E, Breuer N., Berneburg H., Emmelmann H.J., 'On the aerodynamic interference due to the rolling wheels of passenger cars.', SAE 910311, 1991.
- [4] Wickern G., Zwicker K. and Pfadenhauer M., 'Rotating wheels- their impact on wind tunnel test techniques and on vehicle drag result', SAE 970133, 1997.
- [5] Holt, D.J., Underbody aerodynamics: the next area of refinement?, SAE Journal, 1982.
- [6] Cooper K.R., Bertenyi T., Dutil G., Syms J. and Sovran G., 'The aerodynamic performance of under body diffusers', SAE 980030, 1998.
- [7] Cooper K. R., Sovran G. and Syms J., 'Selecting automotive diffusers to maximize underbody downforce', SAE 2000-01-0354, 2000.
- [8] Aronson D., Brahim S.B. and Perzon S., 'On the underbody flow of a simplified estate', SAE 2000-01-0485, 2000.
- [9] Wiedemann J., 'The influence of ground simulation and wheel rotation on aerodynamic drag optimization- Potential for reducing fuel consumption', SAE Tech. paper 960676, 1996.
- [10] Jansn, J., Darrieutort, L., Bannister, M. and Seremak, P., New Development and Working Methods used in the Aerodynamic Development of the New Large estate, JSAE Spring Convention, paper 20005352, 2000.
- [11] Cogotti, A., A Parametric Study on the Ground Effect of a Simplified Car Model, SAE tech. paper 980031, 1998.
- [12] Koike, M., Nagayoshi, T. and Hamamoto, N., "Research on Aerodynamic Drag Reduction by Vortex Generators", MITSUBISHI Motors Technical Review, paper no.16, 2004.
- [13] WANG Jing-yu, LAI Chen-guang and HU Xing-jun "Influence of Automotive Underbody Shape on Aerodynamic Performance", China journal of Highway and Transport, Vol.21 no.2, Mar. 2008.
- [14] DeltaLab., 'Aerodynamic Aspiration EA600 type- Subsonic wind tunnel', Technical Report, Dec. 1996.
- [15] DeltaLab., 'Extensometer bridge, EI616 type', Technical Report, Dec. 1996.
- [16] Iremonger M. J., "Basic stress analysis ", Butter worth publisher, England, 1984.
- [17] Hucho W. H., Emmelmann L. J., "The optimization of body details- A method for reducing the aerodynamic drag of road vehicles", SAE paper 760185, February 1976.
- [18] Gilhaus A., "The main

parameters determining the aerodynamic drag of buses" Colloque Construire avec le vent. Vol.2, Centre Scientifique et Technique du Bâtiment, Nantes, June 1981.

Table (1) Values of drag coefficient obtained in the present work using strain gauge method ($Re=2.8 \times 10^5$ to 6.55×10^5) for all models.

Vehicle Model	One-box Form	Two-box Form	Three-box Form
Mercedes SEL300 Model			0.45
Hyundai Model			0.39
Toyota Model		0.53	
Pajero Model		0.34	
SNVI mini-bus Model	0.68		

Table (2) Values of drag coefficient obtained from using pressure distribution

<i>Vehicle Reference</i>	<i>One-box Form model</i>	<i>Two-box Form model</i>	<i>Three-box Form model</i>
<i>Porsche 924 Turbo</i> [17]			
<i>VW POLO</i> [17]			
<i>Mercedes 500SE</i> [17]			
<i>Citroen GSA</i> [17]			
<i>Sharp-edged Front</i> [18]	 0.88		
<i>Front with Rounded leading Edges</i> [18]	 0.36		
<i>'Stromform'-front</i> [18]	 0.34		

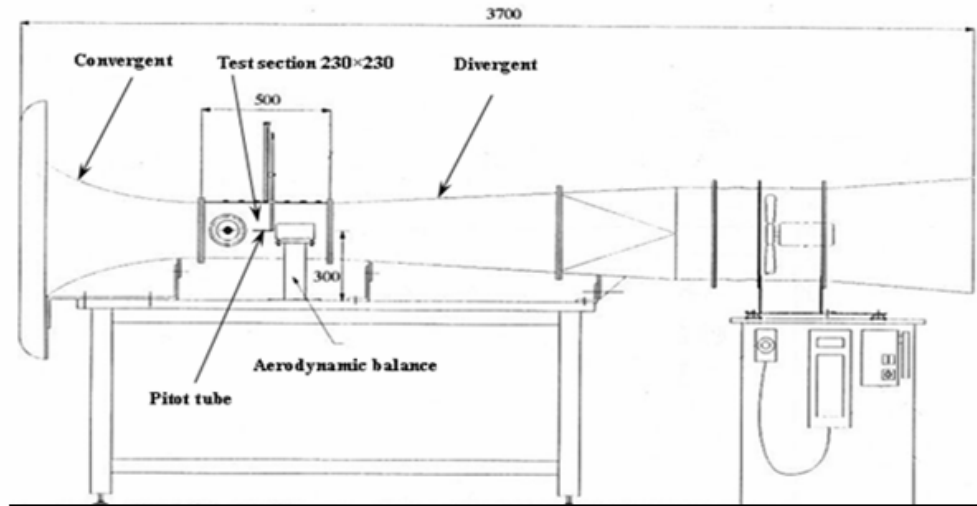


Figure (1) the scheme of wind tunnel [4].

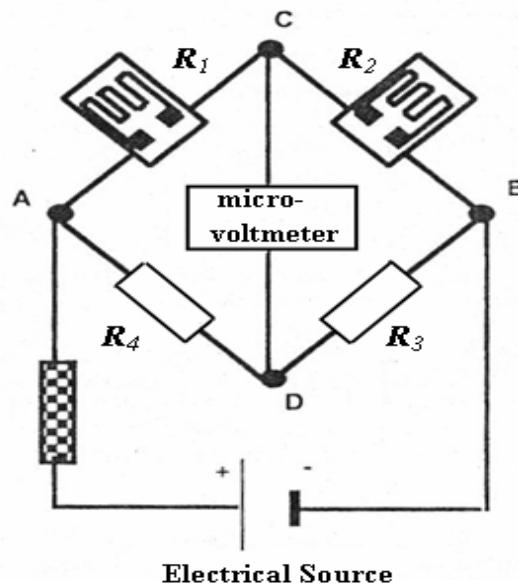


Figure (2) Half bridge connection [5].



Three-box form
Passenger car models

Two-box form
Passenger car models

One-box form
Passenger car model

Figure (3) three, two, and one-box form passenger car models

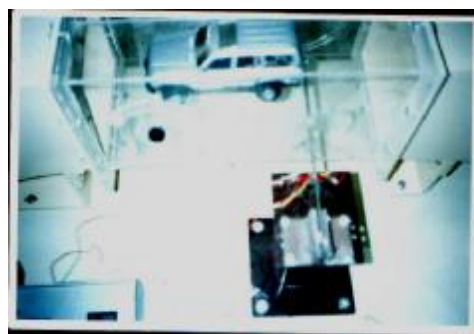
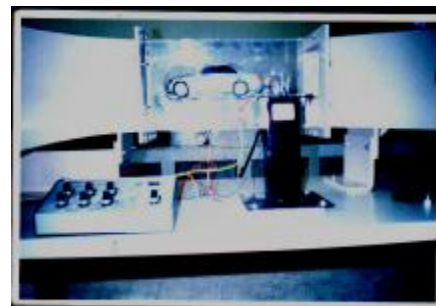


Figure (4) Experimental procedure for Mercedes SEL300, Hyundai, Toyota and Pajero models

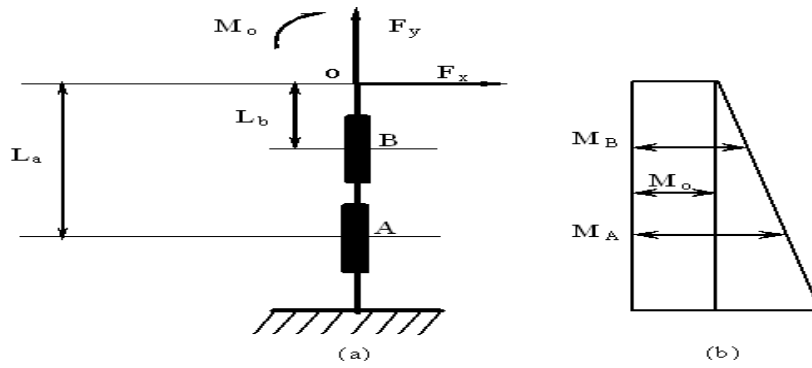


Figure (5) Bending moment diagram for the sting in vertical position.
(a) Vertical position for the sting.

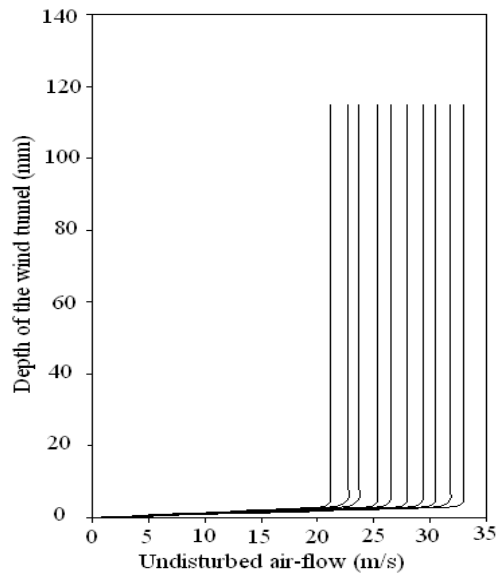
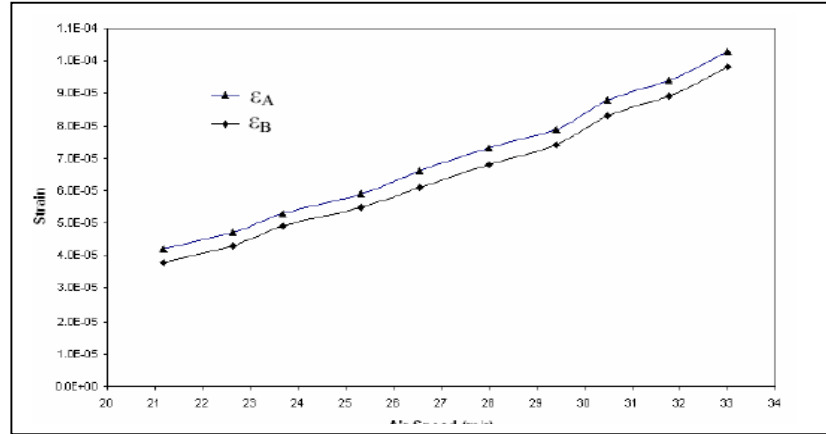
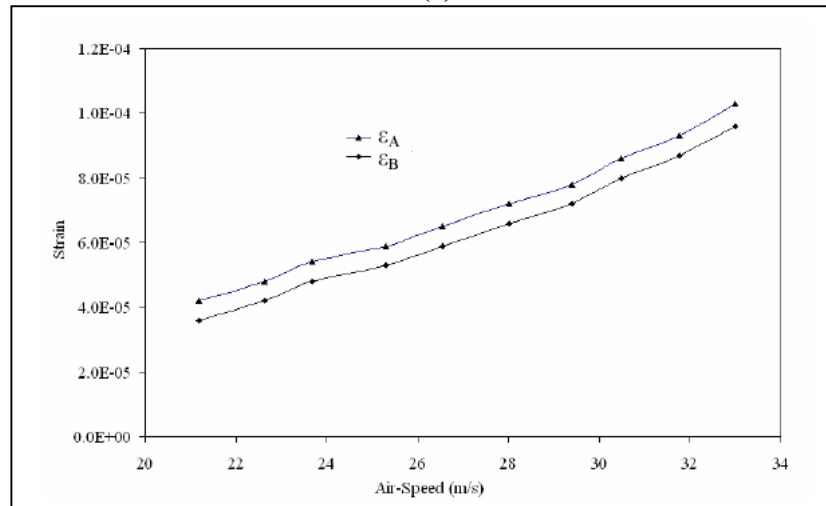


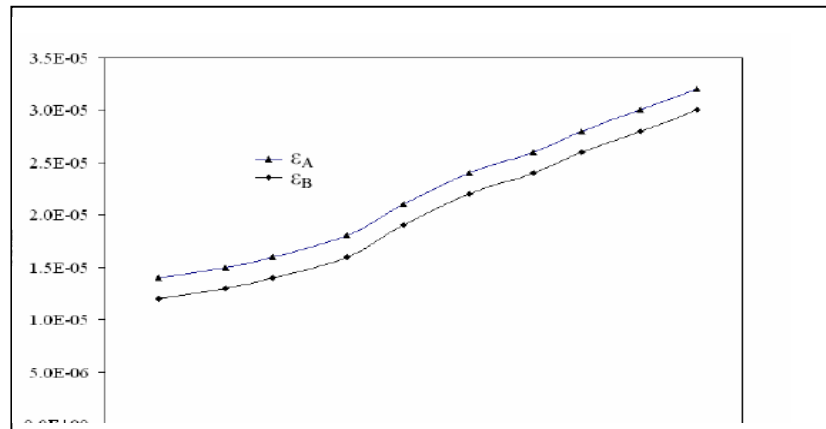
Figure (6) Velocity distribution within the test section.
From calibration of the wind tunnel.



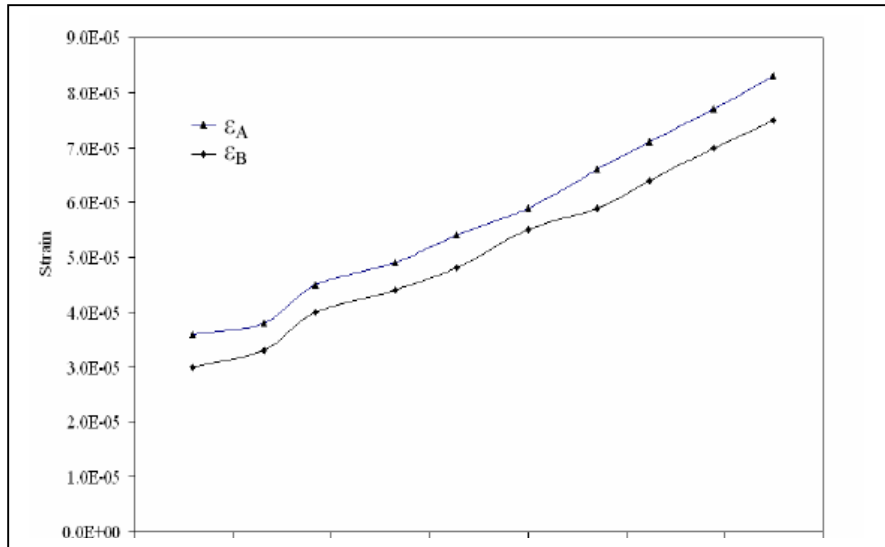
(a)



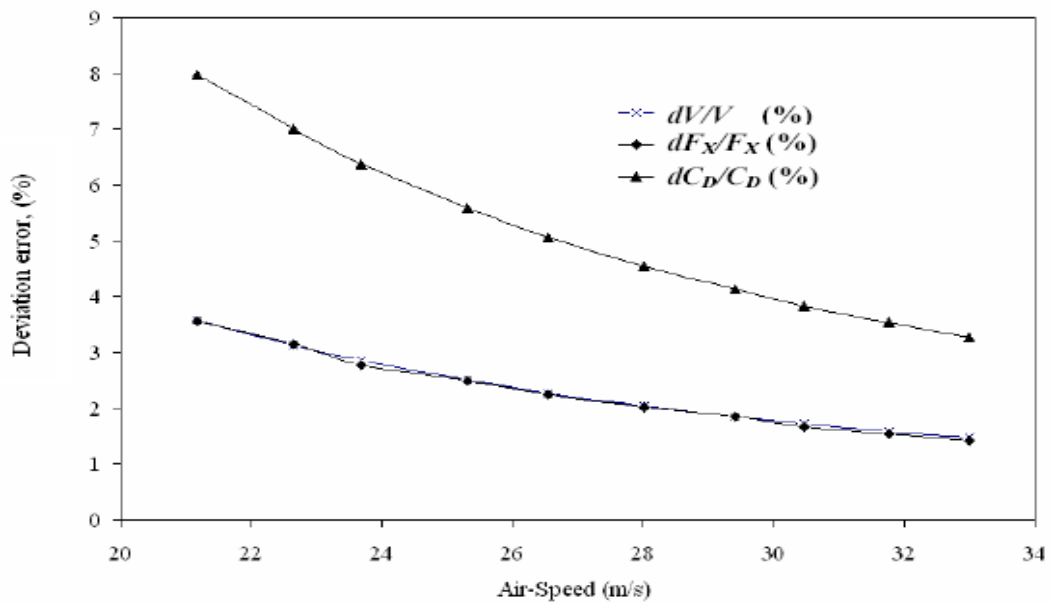
(b)



(c)



(d)



(e)

Figure (7) Variation of strain with an air-speed for (a)Mercedes SEL300 model,(b) Hyundai model (c)Toyota model, (d) Pajero model and (e) SNVI mini-bus model

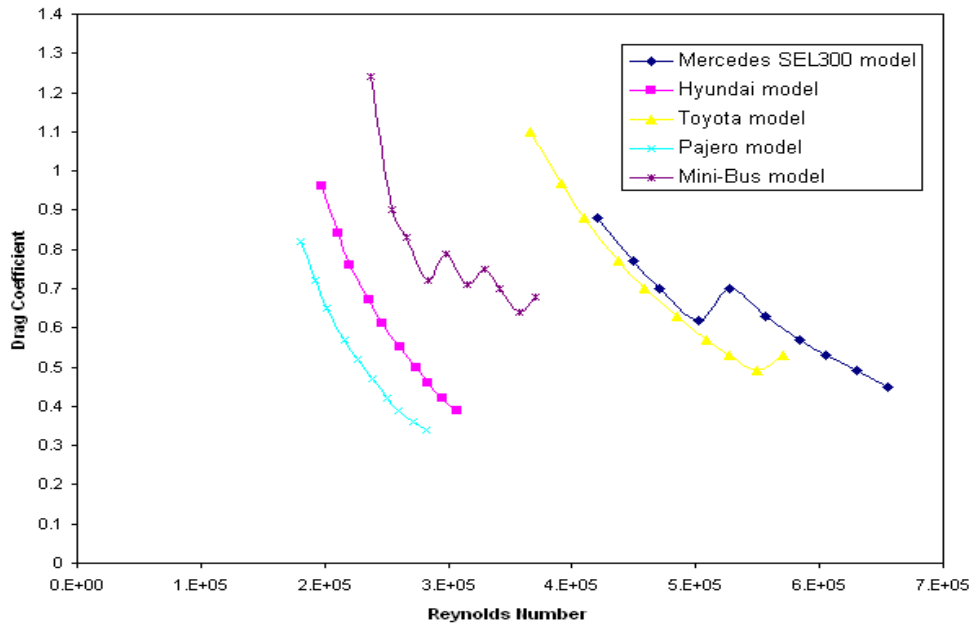
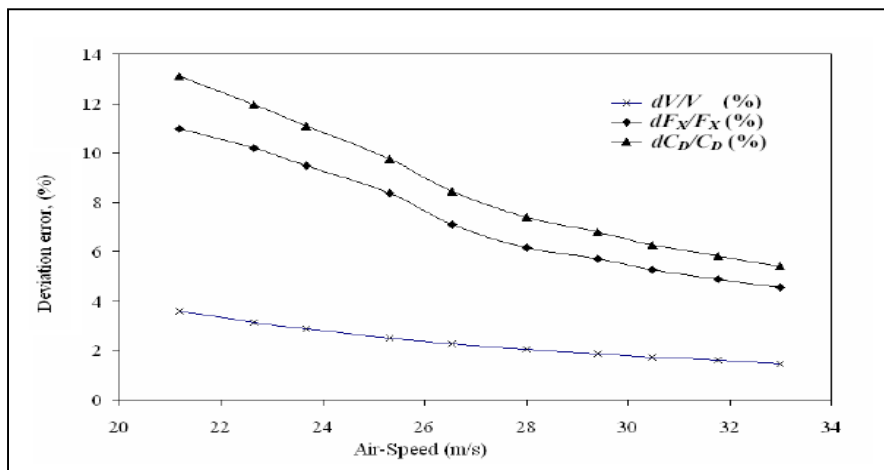
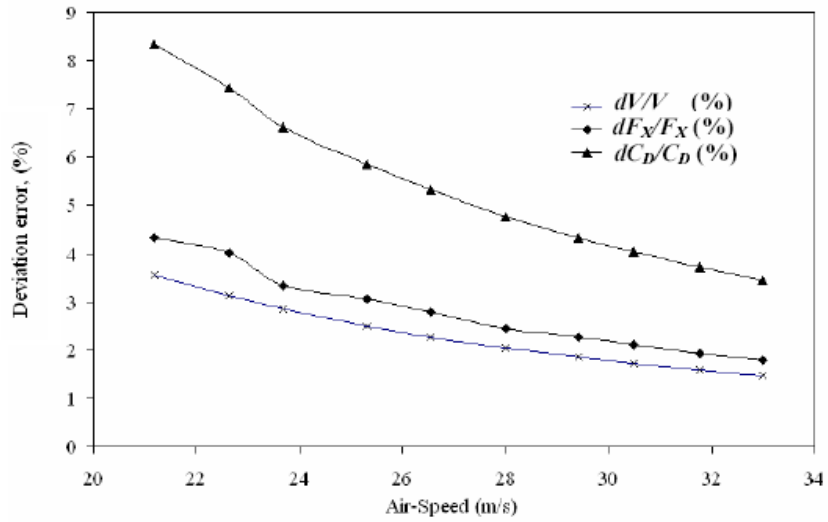


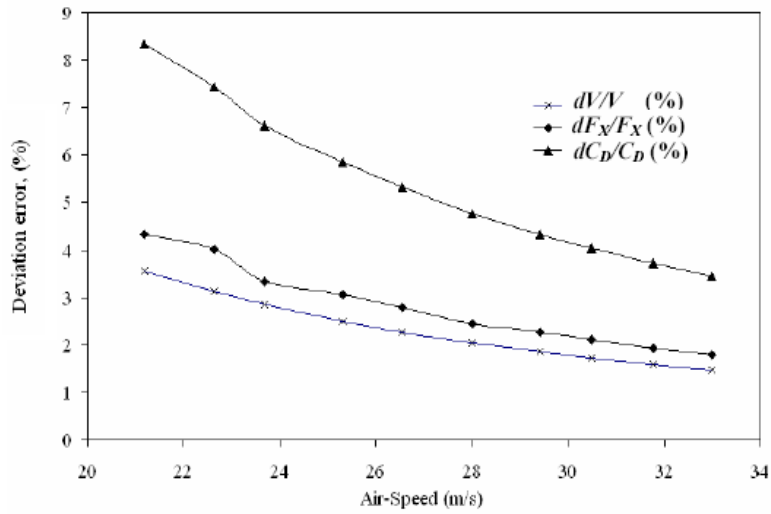
Figure (8) Drag coefficient variation as a function Reynolds number For different vehicles' profiles.



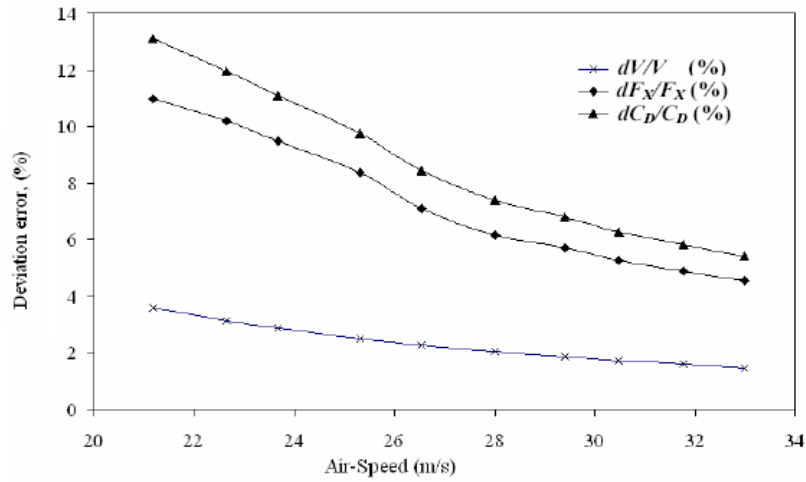
(a)



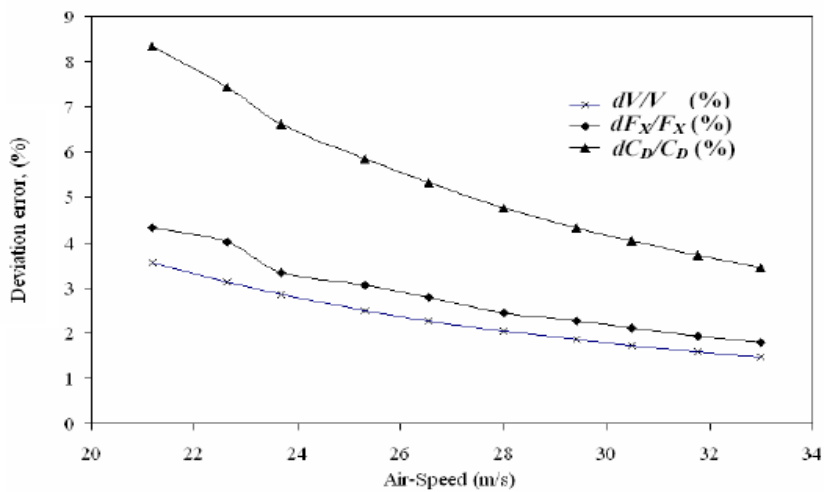
(b)



(c)



(d)



(e)

Figure (9) Variation of deviation errors with an air speed for
 (a) Mercedes SEL300 model
 (b) Hyundai model
 (c) Toyota model
 (d) Pajero model
 (e) SNVI mini-bus model